Scientific Research Publishing

Journal of Power and Energy Engineering, 2025, 13(9), 274-301
https://www.scirp.org/journal/jpee
ISSN Online: 2327-5901
ISSN Print: 2327-588X

Hybrid Singular Parameter Phasor Measurement Based on the Discrete Fourier Transform (DFT)-Adaptive Artificial Neural Network (ADALINE) Algorithm

Gabriel Musonda, Charles Lubobya, Ackim Zulu

Department of Electrical Engineering, School of Engineering, University of Zambia, Lusaka, Zambia
Email: musondagabriel50@gmail.com, ackim.zulu@unza.zm, cslubobya@unza.zm

How to cite this paper: Musonda, G., Lubobya, C. and Zulu, A. (2025) Hybrid Singular Parameter Phasor Measurement Based on the Discrete Fourier Transform (DFT)-Adaptive Artificial Neural Network (ADALINE) Algorithm. *Journal of Power and Energy Engineering*, **13**, 274-301.
https://doi.org/10.4236/jpee.2025.139019

Received: August 17, 2025
Accepted: September 21, 2025
Published: September 24, 2025

Abstract

The PMU's performance relies on its ability to detect and provide accurate measurements of both steady-state and dynamic conditions. The phasor estimation algorithm assesses the accuracy and quality of measuring grid parameters under various operating conditions. The Discrete Fourier Transform (DFT) algorithm is the most commonly used because of its low computational complexity and ease of implementation on any hardware. However, DFT has limitations in accurately obtaining a phasor during off-nominal grid frequency conditions caused by inter-harmonics, intermodulation, and frequency ramps. This paper introduces the design of a Hybrid DFT-ADALINE model. The ADALINE is a linear activation function where the input is directly proportional to the output, and it can learn from its environment and adjust its weights to minimize errors. Recently, many researchers have focused on applying an adaptive linear neural network (ADALINE) for parameter estimation due to its low computational complexity, minimal tracking error, and faster convergence rate. ADALINE is widely used as a harmonic estimator because of its simple structure and ability to track nonstationary signal parameters. A key feature of this approach is the integration of ADALINE, which tracks the estimated frequency and the phase angle error output of the PMU, converting it into a correlation coefficient. The ADALINE deep learning AI analyzes the changing pattern of frequency relative to the nominal grid frequency, comparing it to the phase angle error to determine the average correlation. The model is calibrated so that it reflects the average correlation for frequencies between 49.5 Hz and 50.5 Hz as normal grid conditions, ensuring the PMU does not generate alarms under these off-nominal conditions. This study demonstrates how a single PMU measurement parameter, the correla-

tion coefficient, can be used to predict the behavior of the power grid under dynamic conditions, and how it can trigger grid voltage and frequency adjustments, significantly simplifying the fault detection logic of the power system and reducing computation latency.

Keywords

Phasor Measurement Unit, Discrete Fourier Transform (DFT), Adaptive Linear Neuron Network (ADALINE), Correlation Coefficient

1. Introduction

The PMU is a sensor device that measures electrical quantities such as voltage and current phasors, frequency, and rate of change of frequency (ROCOF), with an accurate time tag based on UTC obtained from a GPS receiver or through IEEE 1588 (Precision Time Protocol) synchronization [1]. Sustained growth in demand, along with unprecedented investments in transmission infrastructure, has led to narrow operational margins for power system operators worldwide. As a result, power networks are operating close to stability limits. This situation has placed significant pressure on power utility companies to explore new avenues for control and protection of wide-area systems [2]. It also necessitates increasing generation through distributed and renewable energy sources. The sudden switching on and off of distributed generators and renewable energy sources introduces a decaying DC offset condition on the grid, which can distort current waveforms and affect the operation of PMUs. Therefore, calculating voltage and/or current phasors, deviation from nominal frequency, and the rate of change of frequency, each with an exact timestamp, supports real-time state estimation and enhances protection schemes [3].

High-performance Phasor Measurement Units (PMUs) are essential for effective monitoring, protection, and control of the power grid, heavily depending on the sensitivity and measurement accuracy of the PMU. These factors are vital for enabling proper control actions that improve the stability and usability of the power system. The performance of the PMU relies on its ability to detect and accurately measure both steady-state and dynamic conditions. It is well-known that the phasor estimation algorithm determines the accuracy and quality of PMU data under various measurement conditions, forming the foundation of all PMU-based technologies and applications [4]. Over time, many algorithms have been proposed to achieve accurate measurement of phasor quantities. However, the Discrete Fourier Transform (DFT) algorithm remains the most widely used because of its low computational complexity, making it implementable on any hardware [5]. DFT offers high frequency resolution, which makes it suitable for precise phasor estimation. As a result, many algorithms developed for phasor measurement are extensions of the DFT. Nonetheless, the measurement accuracy of the DFT algorithm can only be guaranteed at the nominal grid frequency [6]. DFT is

a time-domain estimation technique that analyzes signal samples through time-domain frequency mixers, filters, or other processing methods to obtain the phasor [7]. This design approach for the PMU is vulnerable to false alarms of low-frequency oscillations during off-nominal frequency (time-variant frequency) conditions. A linear relationship exists between the input vector frequency, the average time error, and the phase angle error of the PMU. This relationship can be used to calibrate the PMU for better resistance against off-nominal frequency effects caused by inter-harmonics, intermodulation, and frequency ramps [8]. Therefore, the state estimation problem in the DFT algorithm can be addressed by manipulating this linear relationship among the input vector frequency, the time-variant frequency, and the phase angle error [9].

The rest of this paper is organized as follows: Section I discusses the theoretical foundations of the phasor estimation algorithms used in the PMU. In Section II, research related to tracking the time-varying frequency and its impact on the phase angle error of the PMU is examined. Section III outlines the basic architecture of a phasor measurement device. Section IV explains the theoretical basis of using the average correlation coefficient to track the time-varying frequency and phase angle error. In section V, the implementation and testing of the hardware model of the PMU are detailed. Section VI presents the results of the PMU testing. Finally, conclusions are given in Section VII.

2. Related Work

Real-time power grid state estimation relies on the event detection method employed: these include signal-processing-based, statistical-based, machine-learning-based, and hybrid approaches [10]. Examples of signal processing techniques are the Discrete Wavelet Transform (DWT), Discrete Fourier Transform (DFT), and the Interpolated Discrete Fourier Transform (IDFT). Statistical methods encompass the Gaussian distribution, Principal Component Analysis, Time Series Analysis, Event Classification, and Outlier Detection. Machine learning techniques involve Support Vector Machines (SVM), Artificial Neural Networks (ANN), Decision Trees, k-Nearest Neighbors (k-NN), Adaptive Artificial Neural Network (ADALINE), and Linear Discriminant Analysis (LDA). Hybrid methods combine signal processing and statistical techniques, machine learning and signal processing, or statistical and machine learning approaches.

Antonio Delle Femine *et al.* [11] employed an advanced PMU internal signal processing method using Interpolated Discrete Fourier Transform (IDFT), integrated into a low-cost microcontroller, to synchronize the sampling frequency with the Universal Time Coordinated (UTC) reference. The IDFT could track the grid frequency and the time-varying phase angle error of the PMU. The prototype was tested with a high-performance PMU calibrator, the Fluke 6135A/PMUCAL, and the results showed impaired phasor measurement under dynamic grid conditions.

Hui Li *et al.* [12] employed a two-layer iterative DFT with resampling to esti-

mate frequency under non-steady state grid conditions. The exponential sampling method was used to set the initial sampling frequency during the inner layer of the DFT iteration. The PMU could track the time-variant frequency back to the normal grid frequency based on the Percentage Total Vector Error (%TVE). Frequency tracking was achieved by calculating the mean squared error of the measured frequency, the rate of change of frequency, and the total vector error during continuously changing transient conditions.

Lei Chen *et al.* [13] used statistical exponential functions to model the decaying dc (DDC) component, and the optimal time constant (TC) for the DDC model was determined using an enumeration method. The rate of change of frequency (ROCOF) of the harmonic was estimated with a second-order fitting technique. The use of Shannon's sampling method reduced the harmonic phasor estimation time. This PMU calibration approach enhanced immunity against off-nominal frequency conditions caused by inter-harmonics, intermodulation, and frequency ramps.

Ravi Ponnala *et al.* [14] developed a hybrid DFT method for constant-magnitude phasor calculation with a rotating phase angle to detect faults in the power system based on the Total Vector Error (TVE). In this approach, the %TVE-based fault detection was determined using the reference phasor value. The results indicated that when a fault, disturbance, or frequency change occurred, the %TVE varied; as a result, the change in TVE was reflected in the calculation of the next sample. Phasor calculation often produces large amounts of data that require significant memory, complicating data analysis. To reduce the need for extensive data storage, data was only saved during disturbance conditions. This method minimized data generation, making data analysis easier for post-disturbance assessments and load forecasting.

This work proposes a hybrid signal processing and machine learning approach to improve phasor measurement in the PMU. It leverages the linear relationship between the time-varying frequency and the phase angle error of the PMU to determine the correlation coefficient. The average correlation coefficient is analyzed graphically to check if it exceeds a set threshold for outlier detection. This method enhances the accuracy of phasor measurements under off-nominal frequency and other dynamic grid conditions.

3. Methodology

The methodology of this work outlines five key components: the setup of the PMU based on the DFT algorithm with the TVE, Phasor Magnitude, Phase Angle Error, Frequency Error Average, Rate of Change of Frequency (ROCOF), and the Average Correlation Coefficient measurement. Each of these features is explained in detail in the subsections below. **Figure 1** shows the block diagram of the proposed model.

3.1. Elements of the PMU

The main components of the PMU include a GPS receiver, low-pass filter, analog-

to-digital converter, phase-locked loop, and the microprocessor-based phasor estimation unit.

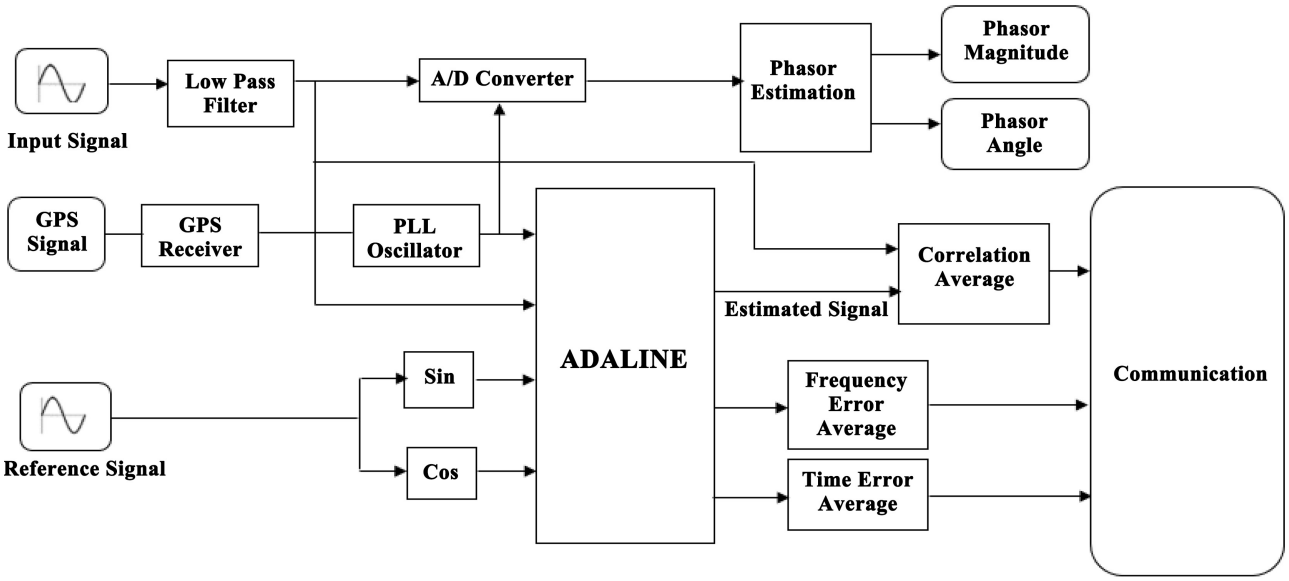

Figure 1. Model block diagram.

The GPS receiver provides the time synchronization signal needed for timestamping measured values. The PLL calculates the phase difference between the input and output signals. The error signal then feeds into the BPF to evaluate the system's stability and overall response [8].

3.2. Band Pass Anti-Aliasing Filter

The transient response of a PMU depends on its filter design. An ideal filter should smoothly attenuate frequencies below the lower cutoff and above the upper cutoff. Filters like Kalman, Gaussian, Butterworth, and Chebyshev are used in PMU applications. The Butterworth filter is known for its flat response in the passband, minimal ripple, and a waveform that can decrease monotonically, with amplitude trends aligned with the diagonal frequency [15]. Conversely, Chebyshev filters—whether analog or digital—have steeper roll-off and exhibit more passband or stopband ripple but offer a less favorable phase response compared to the Butterworth filter [16]. Kalman filters are commonly used for analyzing dynamic systems with normally distributed noise but are less effective for nonlinear systems [17]. Typically, these filters need modifications to handle nonlinear systems effectively. The extended Kalman filter addresses this by linearizing the nonlinear system around a nominal state frequency [18]. To address issues such as non-Gaussian noise and outlier interference, a cubature Kalman filter based on robust functions (RF-CKF) has been proposed [19]. Therefore, the filter design of the PMU should facilitate the linearization of the grid's nonlinear transient conditions so they can be processed effectively by the ADALINE. The IEC/IEEE Standard requires that the PMU's response to a voltage or phase step should have a step re-

sponse with less than 5% overshoot [20].

In this paper, we propose replacing the traditional Low Pass Filter (LPF) with a 4th order Butterworth Band Pass Filter (BPF) in the design of the Hybrid DFT-ADALINE model to enhance the PMUs' response to Poisson-Gaussian noise within the 49.5 Hz to 50.5 Hz pass band. The transfer function of the BPF is shown in Equation (1) below.

$$\left|H\left(j\omega\right)\right|^2 = \frac{1}{1+\left(\frac{\omega^2-\omega_0^2}{\beta_\omega}\right)^{2n}} \tag{1}$$

where $\omega_0 = \omega_L + \omega_H$ is the center frequency, $\beta = \omega_H - \omega_L$ is the bandwidth, $\omega_L = 2\pi fL$ represents the lower cutoff in radians per second, and $\omega_H = 2\pi fH$ represents the upper cutoff in radians per second. The 4th-order Butterworth filter will have a sharp frequency response, as shown in Figure 2 below.

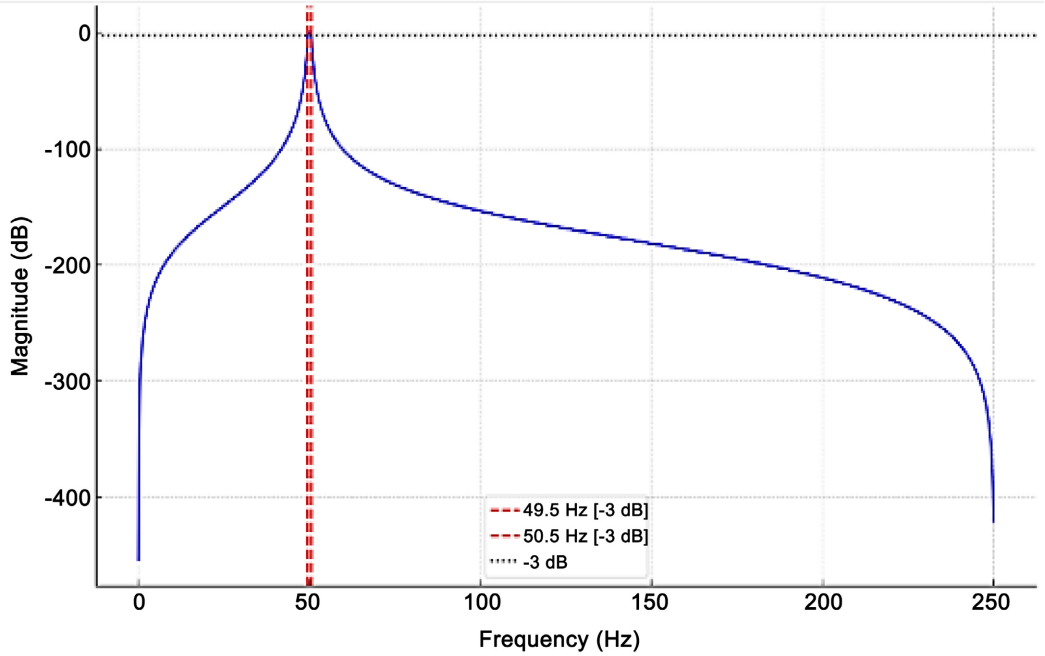

Figure 2. Fourth-order Butterworth bandpass filter frequency response.

The filter design offers excellent noise rejection, minimal signal distortion in the 49.5 Hz to 50.5 Hz pass band, smooth attenuation at the boundaries, and minimal phase distortion.

3.3. Analog to Digital Converter

The ADC converts the analog signals of voltage and current into digital signals for analysis by the microcontroller and extracts valuable information from these signals. The ADC should be fast, operate linearly within the specified region, and have high resolution [21]. The Pulse Per Second (PPS) signal acts as a critical reference for monitoring the local oscillator, which drives the ADC during the sam-

pling process [22].

3.4. Total Vector Error (TVE) and Frequency Error

The TVE results from both magnitude error and phase angle error, derived from the vector that separates the theoretically applied phasor and the estimated phasor. The resulting vector magnitude is normalized by dividing it by the theoretical vector magnitude, producing the TVE [23]. If only one phase is considered, then the total vector error is expressed as in Equation (2) below.

$$\mathrm{TVE} = \frac{\left|X_m - X_n\right|}{\left|X_n\right|} \times 100\% \tag{2}$$

where X_m is the measured vector and X_n is the reference vector. Frequency Error (FE) estimation is calculated using Equation (3) below;

$$\mathrm{FE} = \left|f_m - f_n\right| \tag{3}$$

where f_m is the measured frequency and f_n is the reference (nominal) frequency. Since frequency is mathematically the derivative of the phase angle, the estimated phase angle can be used to determine the original input signal's frequency [24].

3.5. DFT-ADALINE Model

The DFT algorithm is recognized for its low computational complexity and ease of implementation across various hardware types; however, its main drawback is the generation of false alarms during off-nominal frequency conditions. The ADALINE is a linear activation function where the input is directly proportional to the output, and it can learn from its environment and adjust its weights to reduce errors. In recent years, many researchers have focused on applying an adaptive linear neural network (ADALINE) for parameter estimation due to its low computational complexity, minimal tracking error, and faster convergence rate [25]. ADALINE is widely used as harmonic estimator because of its simple structure and nonstationary signal parameter tracking capability. However, when it is applied in the estimation of signals with time-varying parameters, a decaying DC function, high measurement noise, and inter-harmonics, it converges prematurely [26]. Therefore, incorporating a lightweight computation of the coefficient of linear correlation into the ADALINE enhances its online harmonics estimation capability. The hybrid DFT-ADALINE algorithm determines the linear relationship between grid frequency error and phase angle, calibrated to accept a range of frequencies and reject those outside this range. It finds the linear correlation between time/frequency error and the phase angle error of the PMU. In this application, correlation coefficient values range from at least 0.75 up to 0.9974. The passband of 49.5 Hz to 50.5 Hz corresponds to correlation coefficients ranging from 0.8 to 0.9974. As a result, estimated signals with correlation coefficient averages of 0.8 to 0.9974 do not trigger alarms on the PMU. Conversely, input signals with correlation coefficients below 0.8 are considered anomalies and cause alarms. Parallel

ADALINE applications are used to compute the linear correlations of time/frequency error and phase angle error. The ADALINE deep learning algorithm enables the DFT algorithm to operate efficiently on the PMU, thereby overcoming challenges related to dynamic grid conditions.

The DFT-ADALINE algorithm is especially useful for phasor estimation because of its computational efficiency and ability to accurately track grid frequency and timing signals in real-time using the correlation coefficient.

In the PMU architecture, the Analog-to-Digital converter clock is synchronized with the global positioning system (GPS), which provides the 1 pulse per second signal [10]. The Phasor estimator calculates the phasor magnitude and angles. The Phase-Locked-Loop (PLL) circuit detects positive-sequence measurement errors caused by off-nominal frequency conditions resulting from the injection of renewable energy into the grid. This technique allows the PMU to dynamically track the estimated frequency relative to the grid's changing frequency. It therefore acts as a key input to the ADALINE for calculating the Frequency Error Average, Time-Error Average, and the Correlation Coefficient. These functions of the ADALINE can be implemented by deploying a microcontroller that meets the specific hardware and software requirements of the PMU.

3.6. Average Correlation

The average correlation coefficients are derived from the linear relationships established by Equation (4) below.

$$\Delta\varphi_0\left(t_s\right)=\Delta\varphi_{rel}\left(t\right)+2\pi\cdot\Delta f_\tau\left(t\right)\Delta t \tag{4}$$

where $\Delta\varphi_0\left(t_s\right)$ is the variation of the relative phase angle with respect to timestamp shifts, $f\left(t\right)$ denotes the instantaneous frequency of the measured signal at time t, and $\Delta f_\tau\left(t\right)$ is the frequency variation between times t_s and t. The function of the algorithm is to track the signal frequency supplied to the ADALINE by the PLL, based on the time-variant phase angle error output of the PMU, and convert it into a correlation coefficient value. This involves running two parallel ADALINEs to compute the average correlation coefficients. The algorithms for the ADALINEs are presented below;

$$\Delta\varphi_0\left(t_s\right)=\Delta\varphi_{rel}\left(t\right)+2\pi f\Delta t \tag{5}$$

To establish the linear relationship between the phase angle error and the time-varying frequency component, the grid frequency, f is treated as a constant value.

It can be observed that t_s can be updated iteratively using Equation (6) below, where τ is the deviation from the UTC.

$$t_s\left(n+1\right)=t+\Delta\tau$$

$$t_s\left(n+2\right)=t+2\Delta\tau$$

$$t_s\left(n+3\right)=t+3\Delta\tau$$

$$t_s(n+4) = t + 4\Delta\tau$$
$$t_s(n+\cdots) = t + (n+\cdots)\Delta\tau \tag{6}$$

The correlation coefficient average is computed according to the algorithm and Equation (viii) below [8];

$$\delta_{(\varphi_0,t)} = \frac{\sum(\varphi_0 - \varphi_{ref})(t_2 - t_1)}{\sqrt{\sum(\varphi_0 - \varphi_{ref})^2 \sum(t_2 - t_1)^2}} \tag{7}$$

Step 1. Initialize ADALINE with reference phase angle φ_{ref}, shift in UTC, τ, with values ranging from 0.1 to 0.2 seconds to estimate the change in phase angle using Equation (3).

Step 2. Calculate the correlation factor $\delta_{(\varphi_0,t)}$ using Equation (8).

Step 3. Check if the correlation factor $\delta_{(\varphi_0,t)}$ exceeds $\delta_{(\varphi_0,t)} \le 0$.

Step 4. Update Δt using (vii) until the error is minimized.

Step 5. Continue until the maximum number of iterations is reached.

Step 6. Finish.

To establish the linear relationship between the phase angle error and the grid frequency component, the UTC, t, is considered a constant value.

$$\Delta\varphi_0(f_s) = \Delta\varphi_{rel}(t) + 2\pi \cdot \Delta f_\tau(t)t \tag{9}$$

It can be observed that the frequency f can be updated iteratively. The formulas for updating the shift in frequency f by substituting the relative change in frequency Δf in (10) are shown below [5];

$$f_t(n+1) = f + \Delta f_\tau$$
$$f_t(n+2) = f + 2\Delta f_\tau$$
$$f_t(n+3) = f + 3\Delta f_\tau$$
$$f_t(n+4) = f + 4\Delta f_\tau$$
$$f_t(n+\cdots) = f + (n+\cdots)\Delta f_\tau \tag{10}$$

The correlation coefficient average is computed according to the algorithm and Equation (11) below [5];

$$\delta_{(\varphi_0,f)} = \frac{\sum(\varphi_0 - \varphi_{ref})(f_2 - f)}{\sqrt{\sum(\varphi_0 - \varphi_{ref})^2 \sum(f_2 - f)^2}} \tag{11}$$

Step 1. Initialize ADALINE with reference phase angle φ_{ref}, shift in the frequency, Δf_τ with values ranging from −0.5 to 0.5 Hz to estimate the change in phase angle using Equation (9).

Step 2. Calculate the correlation factor $\delta_{(\varphi_0,f)}$ using Equation (11).

Step 3. Check if correlation factor $\delta_{(\varphi_0,f)}$ exceeds $\delta_{(\varphi_0,f)} \le 0$.

Step 4. Update Δf_τ using Equation (x) until the desired error level is achieved.

Step 5. Continue until the maximum number of iterations is reached.

Step 6. Finish.

4. Implementation and Testing

The DFT-ADALINE algorithm is implemented on the PMU in MATLAB/Simulink using the block diagram in Figure 3. Its functionality is validated through frequency ramp tests, magnitude step, and GPS signal loss.

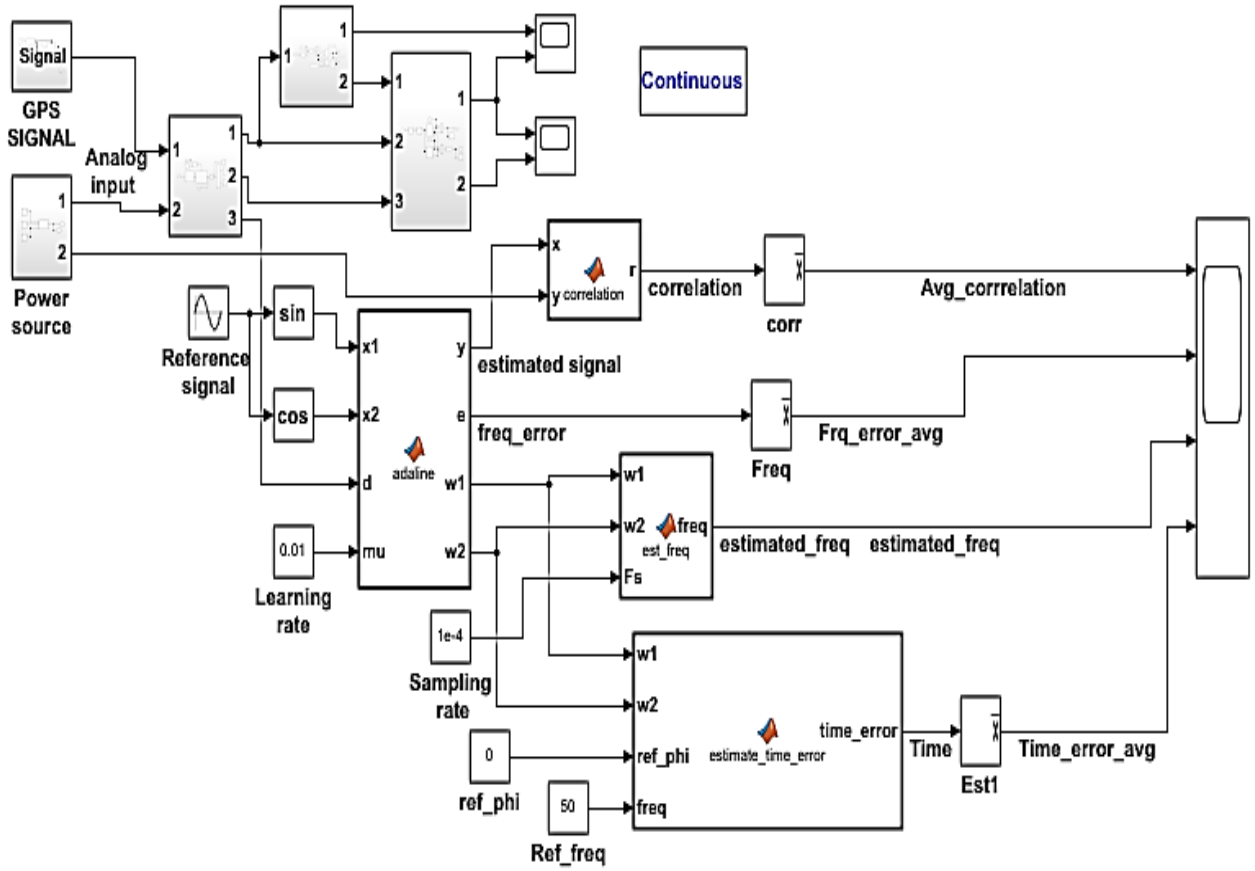

Figure 3. DFT-ADALINE simulink model.

5. Results and Discussion

The results show enhanced performance in the results obtained for the FE, RFE, TE, and TVE compared to the standards set in the IEEE 37.118 for the P-class and M-class PMUs. The results obtained for the PMUs' performance parameters are reflected in a singular parameter called the correlation coefficient.

From 0 to 0.8 s, the measured signal frequency is 49.55 Hz, indicating a deviation of −0.45 Hz from the nominal 50 Hz reference value. The correlation remains one during this period, reflecting steady-state operation of the grid amidst a negative frequency ramp in the measured signal, as shown in Figure 4. Between 0.8 and 1.6 s, the correlation sharply drops to −1 because the measured signal undergoes a 180˚ phase shift relative to the reference signal—phase angle error. The injection of the step signal into the PMU at 0.787 seconds caused a 180˚ phase inversion of the input signal, resulting in the perfect negative correlation detected by the PMU.

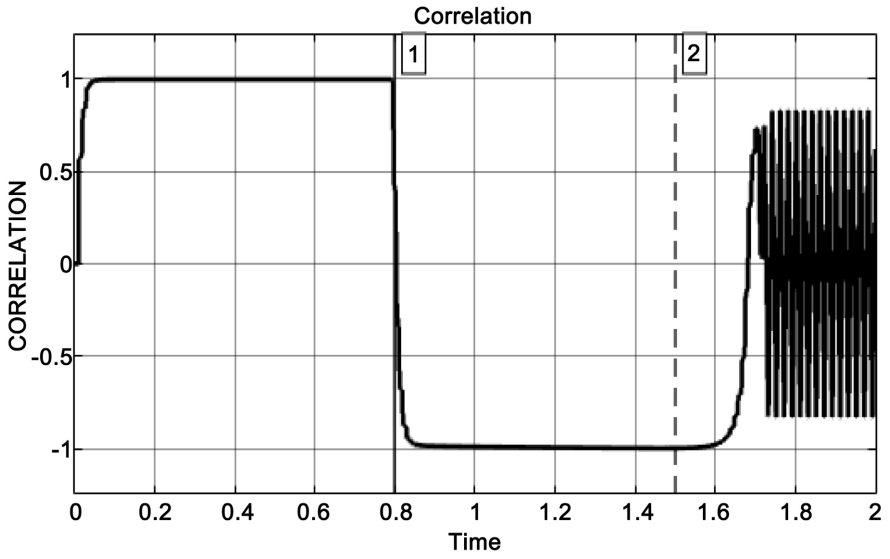

Figure 4. Correlation Average at 49.55 Hz.

Time range (1.6 - 2.0 s): This period indicates a failure of the 1.6 s GPS signal to the PMU. It is evident from the high-frequency oscillations between −1 and +1. The typical shape of the average correlation curve is likely similar under other abnormal conditions, such as noise and processing delays.

From 0 to 0.8 s, the measured signal frequency is 50.00 Hz, indicating a deviation of 0 Hz from the nominal 50 Hz reference value. The correlation remains at one during this period, reflecting steady-state operation of the grid, as shown in Figure 5. Between 0.8 and 1.6 s, the correlation is maintained at +1, despite the measured signal undergoing a 180˚ phase shift relative to the reference signal—zero phase angle error.

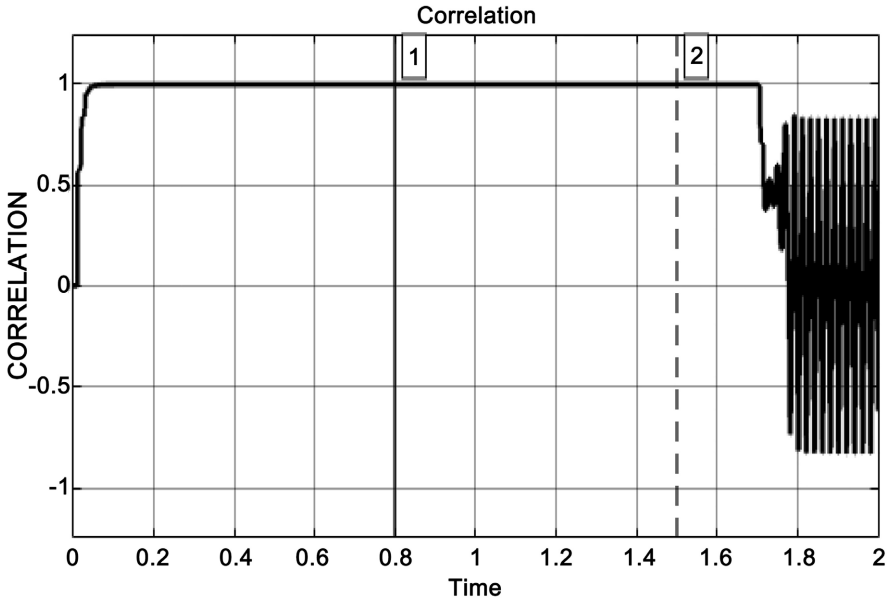

Figure 5. Correlation average at 50.00 Hz.

Time range (1.6 - 2.0 s): This period indicates a failure of the 1.6 s GPS signal to the PMU. It is evident from the high-frequency oscillations between −1 and +1. The typical shape of the average correlation curve is likely similar under other abnormal conditions, such as noise and processing delays.

From 0 to 0.8 s, the measured signal frequency is 50.45 Hz, indicating a deviation of +0.45 Hz from the nominal 50 Hz reference value. The correlation remains one during this period, reflecting steady-state operation of the grid amidst a positive frequency ramp in the measured signal, as shown in Figure 6. Between 0.8 and 1.6 s, the correlation sharply drops to −1 because the measured signal undergoes a 180˚ phase shift relative to the reference signal—phase angle error. The injection of the step signal into the PMU at 0.787 seconds caused a 180˚ phase inversion of the input signal, resulting in the perfect negative correlation detected by the PMU.

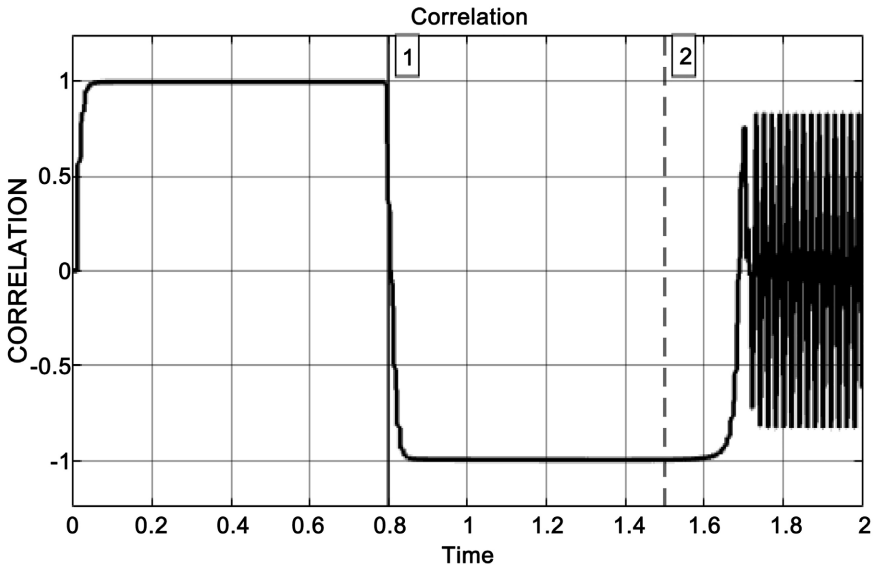

Figure 6. Correlation average at 50.45 Hz.

Time range (1.6 - 2.0 s): This period indicates a failure of the 1.6s GPS signal to the PMU. It is evident from the high-frequency oscillations between −1 and +1. The characteristic of the average correlation curve is likely to be the same for other abnormal conditions, including high-frequency noise or jitter.

From 0 to 0.8 s, in Figure 7, the Time Error is approximately zero, with only a small initial unstable condition before settling. During this period, the internal clock of the PMU is nearly synchronized with the time-variant frequency of the PMU output at 49.55 Hz. As a result, the PMU provides time-stamped measurements with minimal time deviation from the reference signal, and both phase angle error and TVE remain below 1%. From 0.8 to 1.6 s, an abrupt increase in oscillations is observed in the time error due to the introduction of the step signal to the PMU at 0.787 seconds. The application of the 1 pu step signal to the PMU at 0.787 s signifies a severe system disturbance that can lead to frequency deviations,

a phase shift of 180˚, and observed time errors.

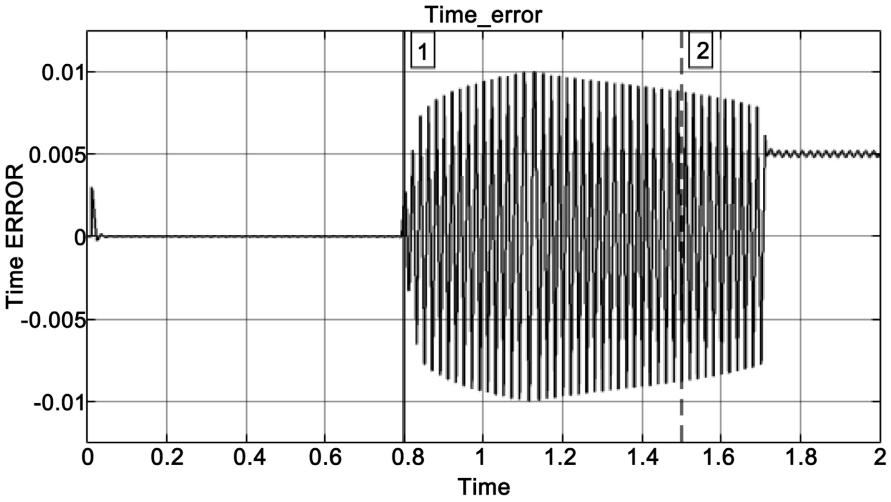

Figure 7. Time error average at 49.55 Hz.

In the time range (1.6 – 2.0 s), the PMU loses the 1.6 s GPS signal and switches to internal clock synchronization, settling at approximately 0.005 s. This indicates an unstable PMU synchronization.

From 0 to 0.8 s, in **Figure 8**, the Time Error is nearly zero, with only a small initial unstable period before stabilizing. During this time, the internal clock of the PMU synchronizes with the time-varying frequency of the PMU output at 50.00 Hz. A minor spike appears at time 0, caused by the system interrupt, but it quickly returns to near zero. This period indicates perfect synchronization of the PMU's internal clock with the reference GPS signal. The input time-varying frequency at 50 Hz matches the reference signal frequency, confirming a zero phase angle time shift, as shown by the zero-time error value.

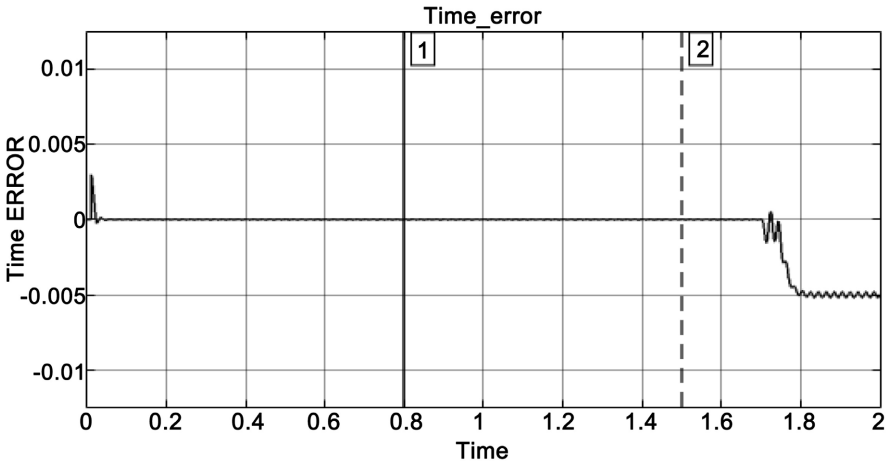

Figure 8. Time error average at 50.00 Hz.

From 0.8 to 1.6 seconds, the time error stays at zero, even though the measured

signal experiences a 180˚ phase shift relative to the reference signal—indicating zero phase angle error.

In the time range (1.6 – 2.0 s), the PMU loses the 1.6 s GPS signal and reverts to internal clock synchronization, settling at approximately 0.005 s. This condition indicates unstable external time-source synchronization for the PMU.

From 0 to 0.8 s, in Figure 9, the Time Error is approximately zero, with only a small initial unstable condition before settling. During this period, the internal clock of the PMU is nearly synchronized with the time-variant frequency of the PMU output at 50.45 Hz. As a result, the PMU provides time-stamped measurements with minimal time deviation from the reference signal, and both phase angle error and TVE remain below 1%. From 0.8 to 1.6 s, an abrupt increase in oscillations is observed in the time error due to the introduction of the step signal to the PMU at 0.787 seconds. The application of the 1 pu step signal to the PMU at 0.787 s signifies a severe system disturbance that can lead to frequency deviations, a phase shift of 180˚, and observed time errors.

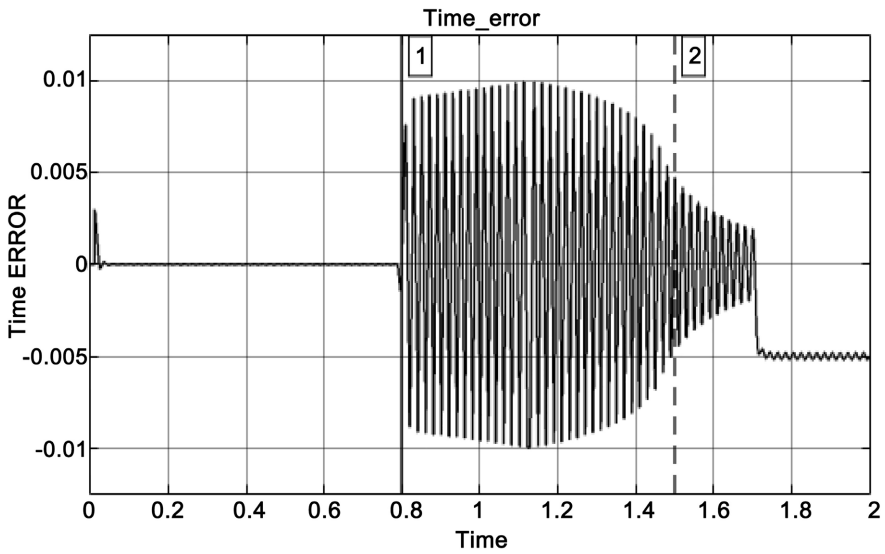

Figure 9. Time error average at 50.45 Hz.

In the time range (1.6 - 2.0 s), the PMU loses the 1.6 s GPS signal and switches to internal clock synchronization, settling at approximately 0.005 s. This indicates an unstable PMU synchronization.

From 0 to 0.8 s, in Figure 10, the frequency error is nearly zero, with minor oscillations, but shows overall perfect synchronization between the measured signal (49.55 Hz) and the reference signal. The near-zero frequency error indicates accurate and steady frequency measurements, with the PMU algorithm functioning optimally.

The 0.8 - 1.6 s period is highly dynamic. After the 1 pu, the step signal is applied to the PMU at 0.787 s, causing a severe frequency error, which is shown by the conical envelope on the curve. During this region, the error increases, reaches a peak, and then decreases symmetrically; the error amplitude peaks at ±0.5 Hz,

equivalent to a TVE of 1%. The zero crossing on the characteristic curve indicates the PMUs' effort to counteract the disturbance caused by the application of the 1 pu step signal.

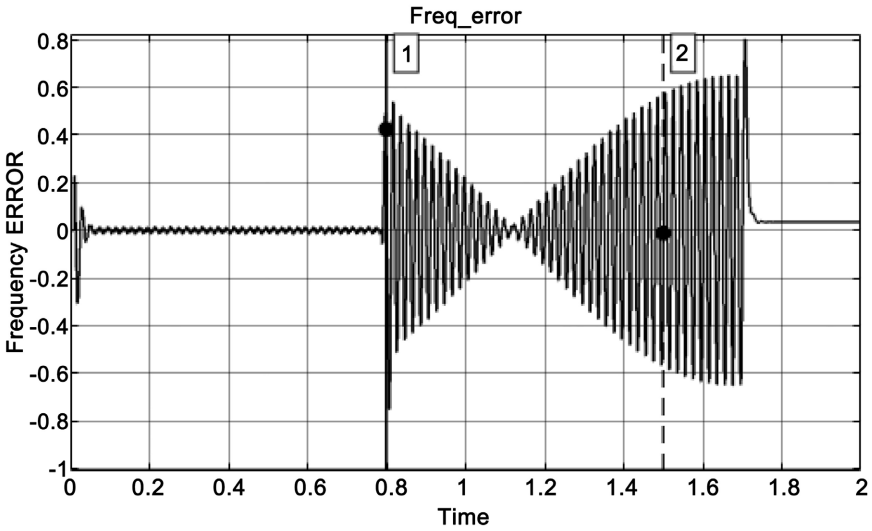

Figure 10. Frequency error average at 49.55 Hz.

Between 1.6 and 2 seconds, the PMU loses the 1.6 s GPS signal. The frequency error then resets to nearly zero, indicating it no longer tracks the signal with the external time source.

From 0 to 0.8 s, in Figure 11, the frequency error is approximately zero, with minor frequency oscillations, but shows overall perfect synchronization of the measured signal (50.00 Hz) and the reference signal. The frequency error being essentially zero indicates perfect and steady frequency measurements, with the PMU algorithm performing optimally.

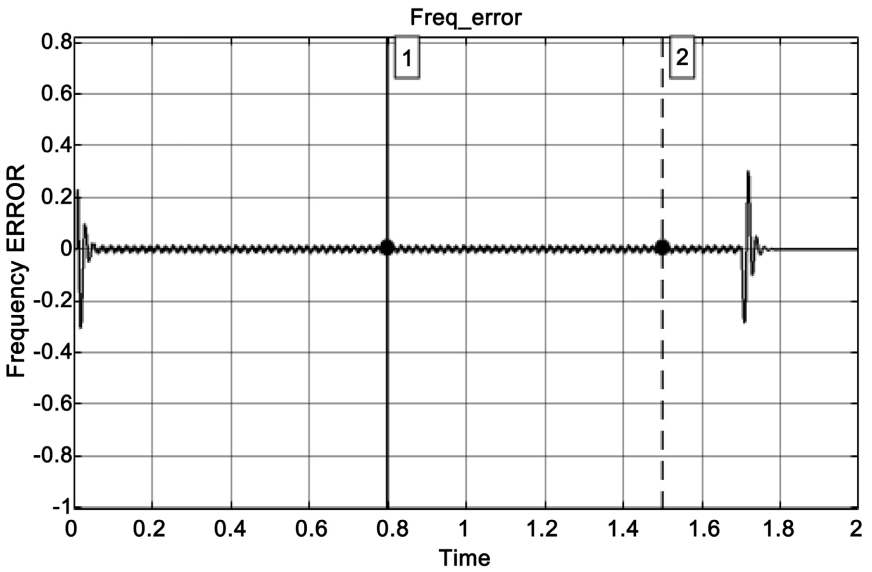

Figure 11. Frequency error average at 50.00 Hz.

From 0.8 to 1.6 seconds, the 1 pu input vector frequency is 50 Hz, so the frequency error is nearly zero. There are negligible, almost undetectable fluctuations around the zero line, indicating highly accurate and stable frequency measurements during this period. The system response shows that even applying the 1 pu step signal to the PMU does not cause a significant frequency error. The input time-variant frequency at 50 Hz matches the reference signal frequency, resulting in a zero phase angle time shift in the zero-frequency error value.

The region 1.6 - 2.0 s indicates the loss of the 1.6 s duration GPS signal to the PMU. This condition is marked by a sudden, sharp rise in frequency error, followed by significant oscillations. A rapid and substantial deviation in the measured frequency occurs, quickly reaching a peak positive error of 0.3 Hz, which corresponds to a TVE of 0.6%, and then decreases to a negative error equivalent to a TVE of 0.4%.

From 0 to 0.8 s, in Figure 12, the frequency error is nearly zero, with minor frequency oscillations, but it shows overall perfect synchronization of the measured signal (50.45 Hz) and the reference signal. The frequency error being essentially zero indicates accurate and steady frequency measurements, with the PMU algorithm performing optimally.

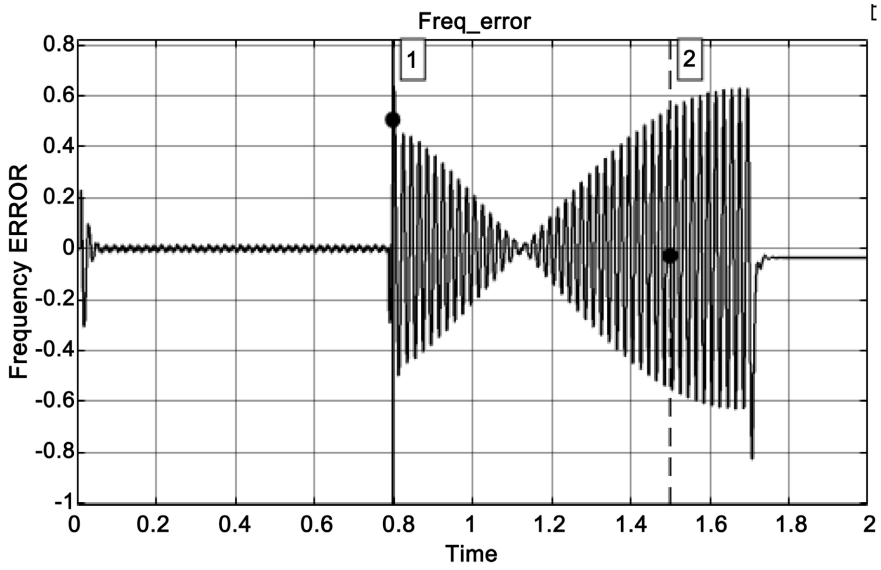

Figure 12. Frequency error average at 50.45 Hz.

From 0.8 to 1.6 seconds, the 1 pu step signal is applied to the PMU at 0.787 seconds, causing a 180˚ phase shift in the PMU output. Significant oscillations are observed at 0.8 seconds after applying the 1 pu step signal to the PMU. The oscillations, initially at 0.4 Hz, seem to settle to zero before increasing to 0.5 Hz, indicating a worsening of the frequency error (TVE = 1%).

During the time range (1.6 - 2.0 s), a GPS signal lasting 1.6 seconds is removed; the frequency error resets to a value near zero, indicating that it is no longer tracking the signal with the component of the external time source.

From 0 to 0.8 seconds, in Figure 13, the estimated frequency remains at the nominal value of 50 Hz, even though the input vector is off-nominal. For an input vector frequency of 49.55 Hz, the TVE is 0.9%, and the average correlation at that value is +1; therefore, the estimated frequency is considered 50 Hz during 0 - 0.8 s, indicating a normal PMU response.

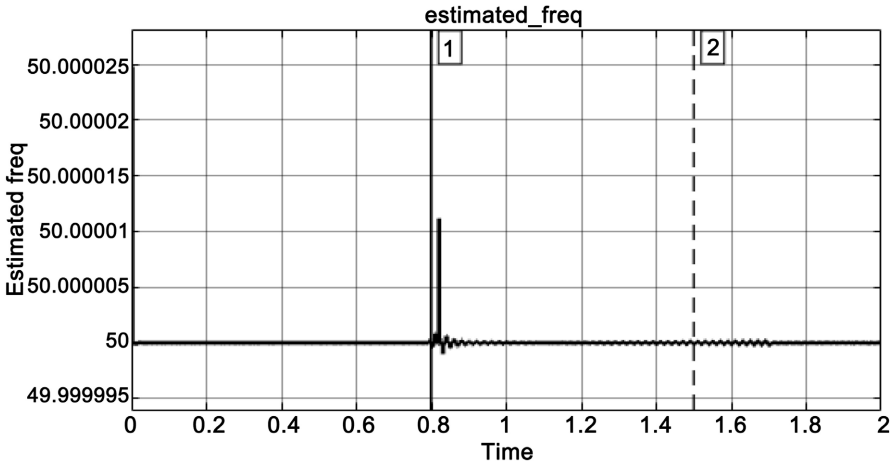

Figure 13. Estimated frequency at 49.55 Hz.

At 0.787 s, a 1 pu step signal is applied to the PMU, causing a frequency spike of about 0.0001. This spike results in a TVE below 0.1%. However, the correlation coefficient in Figure 4, recorded under the same conditions, shows a quick drop in the average correlation coefficient to −1, due to a 180˚ phase inversion caused by the step signal. The estimated frequency remains around the 50 Hz threshold, with some oscillations visible after the GPS signal to the PMU is removed.

The estimated frequency curve of Figure 14 is relatively constant throughout the entire signal duration, except after the 1.7 s mark, where some visible oscillations appear due to the withdrawal of the GPS signal.

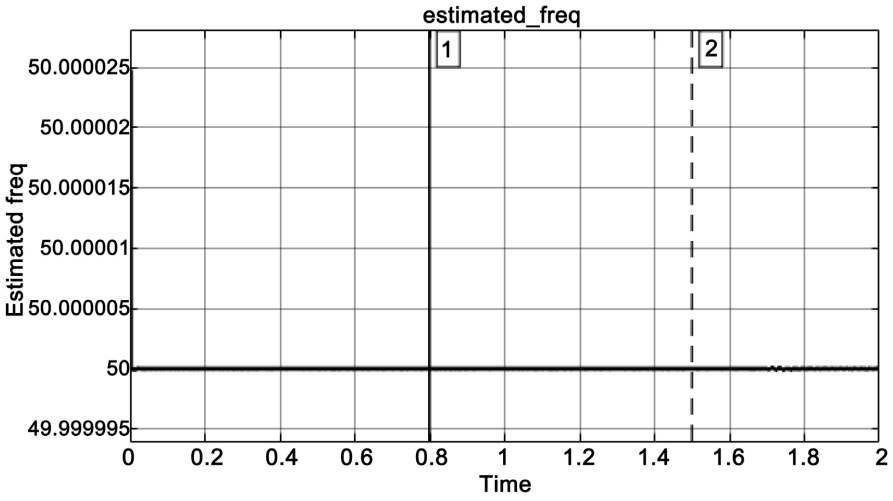

Figure 14. Estimated frequency at 50.00 Hz.

The estimated frequency curve in Figure 15 shows that for the 1 pu, 50.45 Hz vector input to the PMU, the estimated frequency remains close to the nominal 50 Hz, even though the input vector is off-nominal. With an input frequency of 50.45 Hz, the TVE is 0.9%, and the average correlation at this value is +1. Therefore, the estimated frequency is considered 50 Hz during the period 0 - 0.8 s, indicating a normal PMU response to the grid conditions.

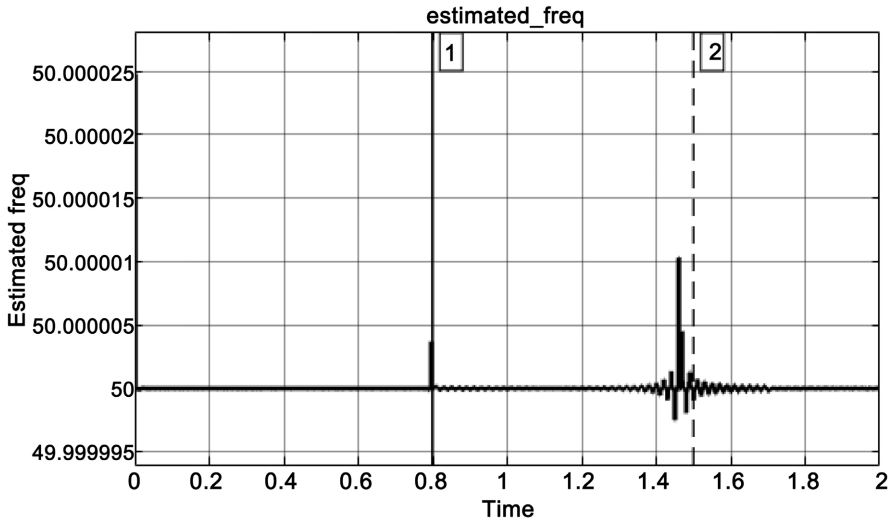

Figure 15. Estimated frequency at 50.45 Hz.

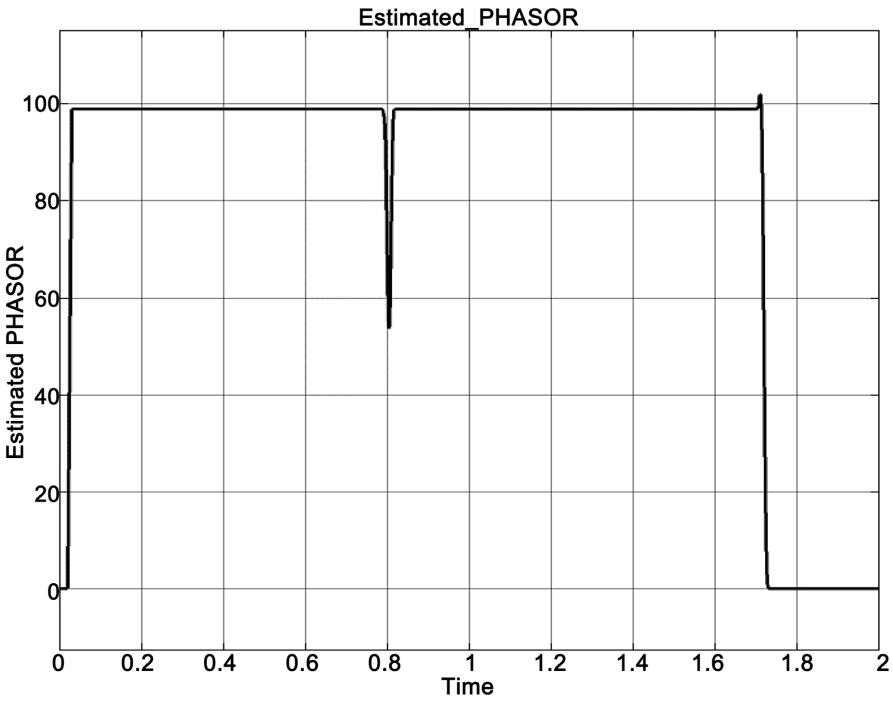

Figure 16. Phasor magnitude at 49.55 Hz.

At 0.787 seconds, a 1 pu step signal is applied to the PMU, causing a frequency spike of approximately 0.0000025. The frequency spike results in a TVE of less

than 0.1%. However, the correlation coefficient in Figure 4 obtained under the same conditions, drops rapidly to −1 due to the 180˚ phase inversion caused by the step signal. At 1.5 seconds, a spike of amplitude 0.000001 appears in the estimated frequency, likely due to the delayed response of the PMU to the step signal. The estimated frequency remains around 50 Hz afterward, but some oscillations are visible after the GPS signal is withdrawn from the PMU.

The estimated phasor magnitude of Figure 16 shows that for the 1 pu, 49.55 Hz vector input to the PMU, the estimated phasor magnitude rises from 0 and rapidly increases to 100, indicating a swift response to the change in the measured signal and remains fairly constant at approximately 100 pu, indicating steady-state operation in the period, 0 - 0.8 s.

The GPS signal to the PMU is removed after 1.6 s, and this is depicted on the graph by the sharp drop in the estimated phasor magnitude to zero, indicating a loss of synchronization.

The estimated phasor magnitude of Figure 17 shows that for the 1 pu, 50.00 Hz vector input to the PMU, the estimated phasor magnitude rises from zero and quickly increases to 100, indicating a rapid response to the change in the measured signal and remains relatively constant at approximately 100 pu, indicating steady-state operation during the period 0 - 1.6 s.

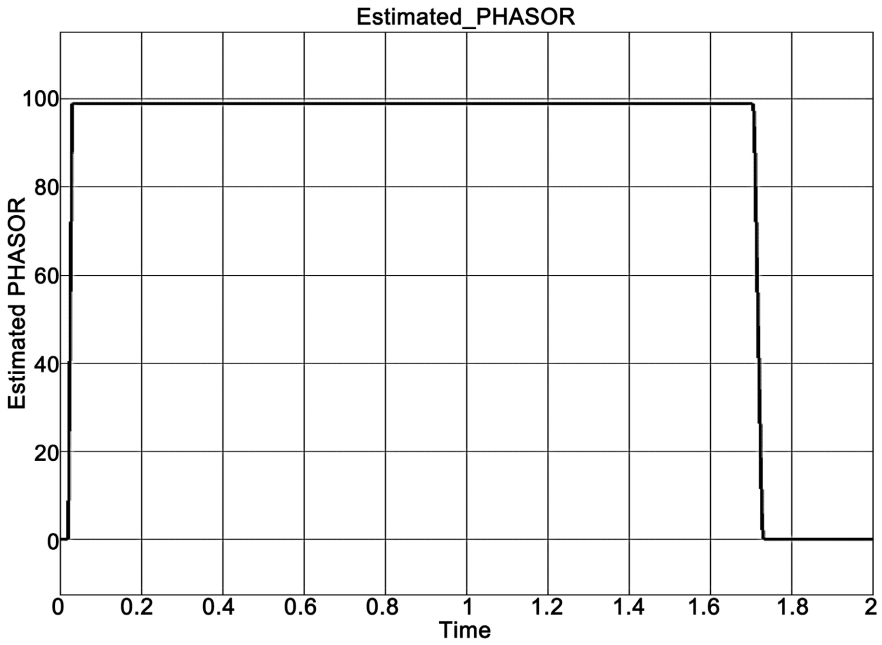

Figure 17. Phasor magnitude at 50.00 Hz.

The GPS signal to the PMU is lost after 1.6 seconds, as indicated by a sharp drop in the estimated phasor magnitude to zero on the graph, which signifies a loss of synchronization.

The graph of Figure 18 shows that for the 1 pu, 50.45 Hz vector input to the PMU, the estimated phasor magnitude rises from 0 and rapidly increases to 100,

indicating a swift response to the change in the measured signal and remains relatively constant at approximately 100 pu, indicating steady-state operation in the period, 0 - 0.8 s.

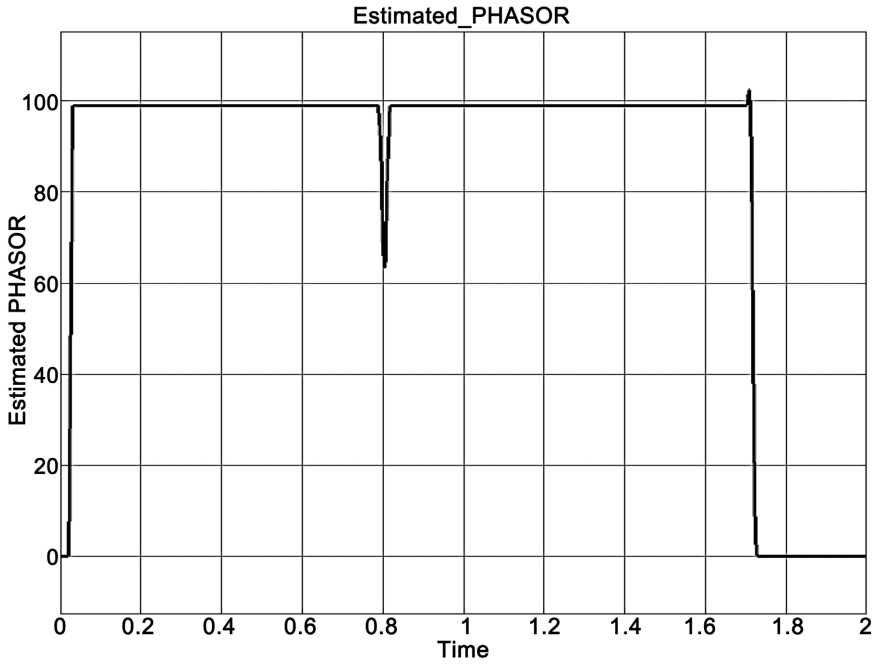

Figure 18. Phasor magnitude at 50.45 Hz.

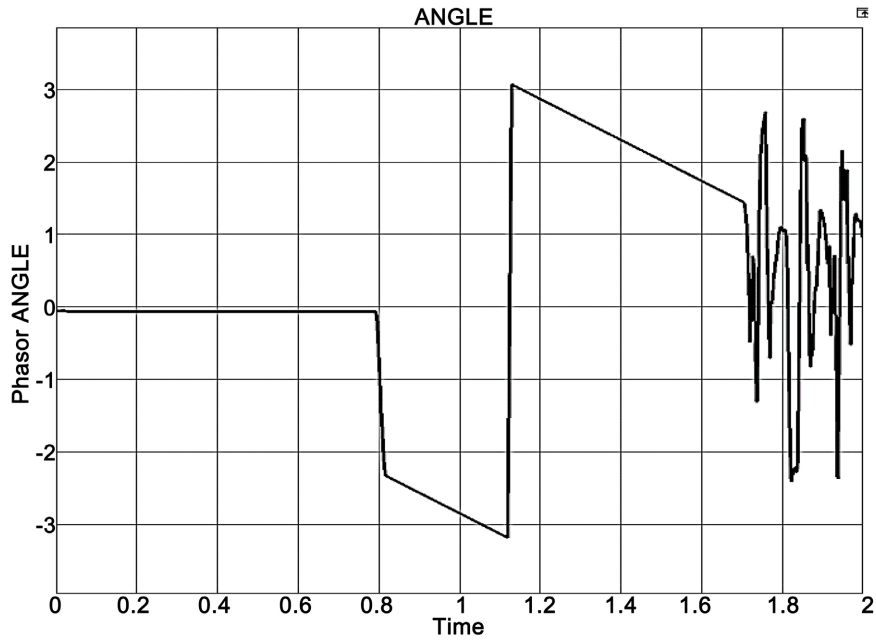

Figure 19. Phase angle at 49.55 Hz.

A sudden dip in amplitude to 65 units occurs in the period 0.79 - 0.81 seconds due to the application of the 1 pu step signal to the PMU. This transient event results in a TVE of 35%, corresponding to a correlation coefficient of −1, as shown

for the same input vector in Figure 18 above.

The GPS signal to the PMU is lost after 1.6 seconds, which is shown on the graph by a sudden drop in the estimated phasor magnitude to zero, indicating a loss of synchronization.

The graph in Figure 19 illustrates that, for the 1 pu, 49.55 Hz vector input to the PMU, the estimated phasor angle remains nearly constant and smooth, indicating that the system is in steady-state and synchronized, with a phase angle approximately at 0 radians during the period 0 - 0.8 seconds.

A sharp drop in the phase angle occurs after the step signal is applied at 0.787 s to the PMU, reaching a minimum near $-\pi$ and indicating a rapid phase shift between 0.8 and 1.2 seconds. Then, the angle quickly increases, overshooting to about $+\pi$, revealing a transient oscillatory response from 1.2 to 17 seconds.

System instability ensues after the removal of the 1.6s duration GPS signal, as can be seen from 1.7 - 2.0 s.

The graph of Figure 20 shows that for the 1 pu, 50.00 Hz vector input to the PMU, the estimated phasor angle is almost constant and smooth, indicating that the system is in steady-state and synchronized, with the phase angle value approximately 0 radians, in the period 0 - 1.7 s. The application of the step signal to the PMU at 0.787 s does not cause any significant measurement error to the phase angle.

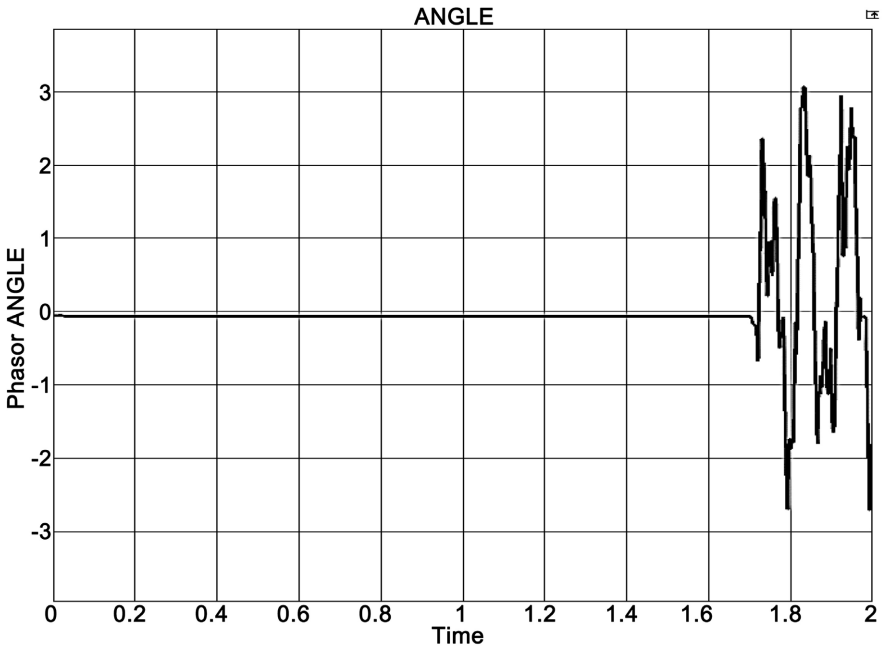

Figure 20. Phase angle at 50.00 Hz.

System instability ensues after the removal of the 1.6 s duration GPS signal, as can be seen from 1.7 - 2.0 s.

The graph in Figure 21 shows that, for the 1 pu, 50.45 Hz vector input to the PMU, the estimated phasor angle remains nearly steady and smooth, indicating

the system is in a steady state and synchronized, with the phase angle approximately 0 radians during the period 0 - 0.8 s.

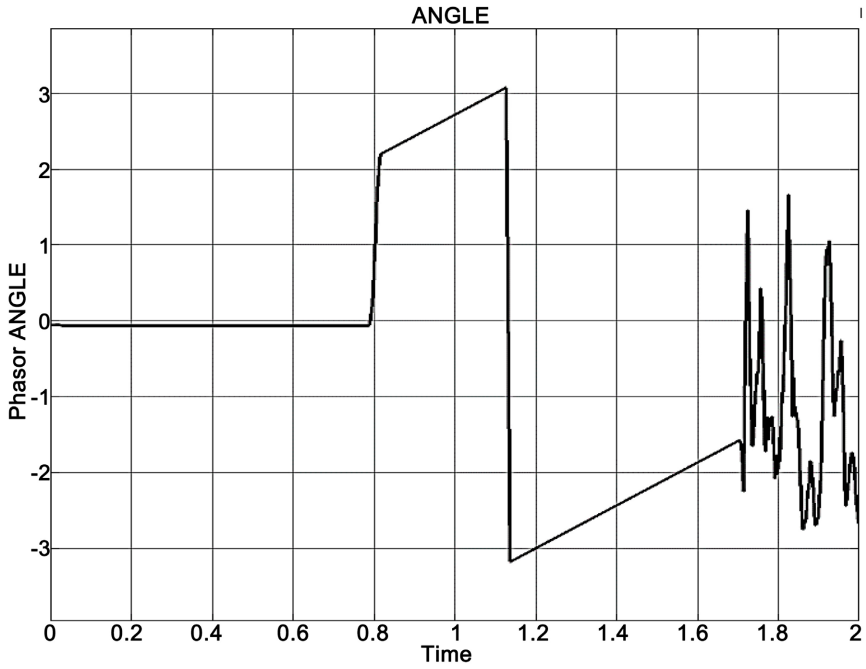

Figure 21. Phase angle at 50.45 Hz.

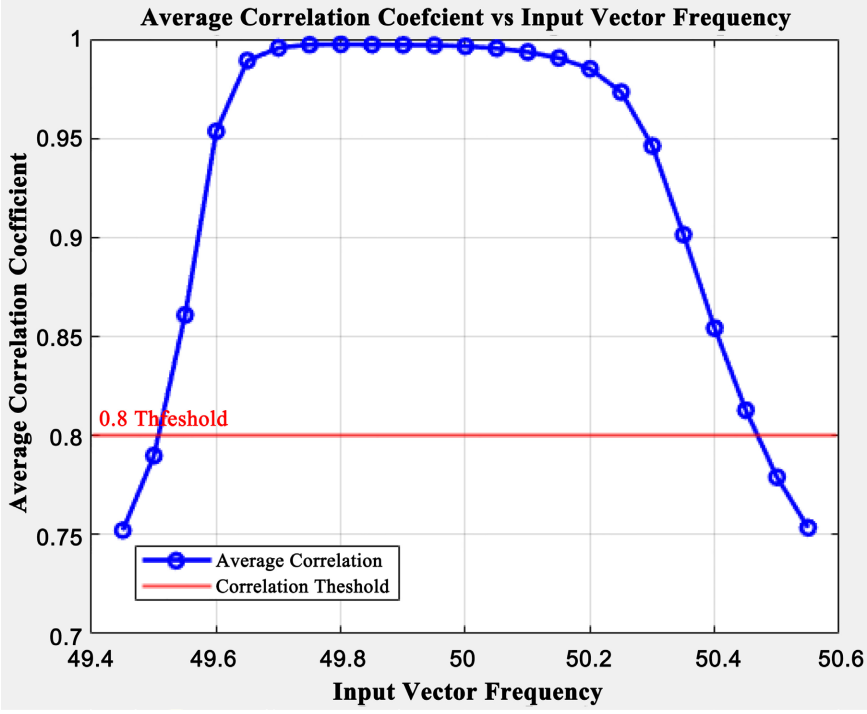

Figure 22. Input vector frequency vs. average correlation coefficient.

A sharp drop in the phase angle occurs after the step signal is applied at 0.787 s to the PMU, reaching a minimum near $+\pi$ and indicating a rapid phase shift be-

tween 0.8 and 1.2 seconds. After this, the angle quickly rises, overshooting to approximately −π, showing a transient oscillatory response from 1.2 to 17 seconds.

System instability ensues after the removal of the 1.6 s duration GPS signal, as can be seen from 1.7 - 2.0 s.

The graph in Figure 22 shows that the average correlation at 49.45 Hz is low at about 0.75, then steadily increases, reaching its peak in the range of 49.80 - 49.85 Hz with a maximum correlation coefficient of 0.9974. Beyond this peak, the correlation coefficient gradually declines to 0.7535 at 50.55 Hz. The graph is symmetric around the 0.9974 peak, indicating a smooth system response near the optimal operating point. The highest correlation zone is approximately between 0.996 and 0.997, covering a narrow band just below the 50 Hz threshold, which represents the most reliable region for the system. Outside the 49.60 - 50.30 Hz range, the correlation decreases more rapidly, showing a fall-off in system performance [8].

5.1. Frequency Ramp Test

In Table 1, the TVE measurements obtained for different frequency ramp test values are presented. The tests for the frequency were conducted within ±0.45 Hz deviations, with a "0 - 0.8" range reported in the table. The TVE% was nearly 0%, with minor spikes (0.004% - 0.006%) in the range ±0.15 to 0.25 Hz, results that are well within the IEEE 37.118 standards' ≤ 3% TVE limit. The readings for the Correlation Coefficient (CC) were exactly 1, indicating perfect linear correlation between measured and reference signals. The Frequency Error (FE) and the Rate of Change of Frequency (RFE) reached maximum values of 0.004 Hz and 0.004 Hz/s, respectively, indicating a steady ramp free of unexpected frequency spikes. The Phasor Magnitude remained constant at 100 pu throughout the tests, and the Phase Angle error was consistently small (±0.05 rad), symmetrical for positive and negative ramps.

Table 1. Compliance signals.

Test condition	Range (Hz)	Period	TVE%	Correlation coefficient (CC)	Frequency error (FE)	Rate of change of frequency (RFE) Hz/s	Phasor magnitude	Phase angle error (PAE)
Frequency ramp	−0.45	0 - 0.8	0	1	0.0039	0.0039	100	0.05
	−0.35	0 - 0.8	0	1	0.0033	0.0033	100	0.05
	−0.25	0 - 0.8	0	1	0.0031	0.0031	100	0.04
	−0.15	0 - 0.8	0.004	1	0.002	0.002	100	−0.05
	0	0 - 0.8	0	1	0	0	100	0
	+0.15	0 - 0.8	0.004	1	0.002	0.002	100	−0.05
	+0.25	0 - 0.8	0.006	1	0.003	0.003	100	−0.04
	+0.35	0 - 0.8	0	1	0.0032	0.0032	100	0.04
	+0.45	0 - 0.8	0.1	1	0.004	0.004	100	0.05
IEEE 37.118			3%		0.005	0.01		

Continued

Step change	1 pu	0.78 - 1.6	1.2	−1	0.6	0.5	100	−π, π
	1 pu	0.78 - 1.6	1.1	−1	0.55	0.55	100	−π, π
	1 pu	0.78 - 1.6	1	−1	0.5	0.5	100	−2.6
	1 pu	0.78 - 1.6	0.8	1	0.4	0.4	100	−1.6
	1 pu	0.78 - 1.6	0	1	0	0	100	−0.02
	1 pu	0.78 - 1.6	0.8	1	0.4	0.4	100	1.5
	1 pu	0.78 - 1.6	0.8	−1	0.5	0.4	100	2.5
	1 pu	0.78 - 1.6	1.1	−1	0.55	0.5	100	π, −π
	1 pu	0.78 - 1.6	1	−1	0.6	0.6	100	π, −π
IEEE 37.118			0.595		0.869	1.038		
No GPS	1 pu	1.6 - 2.0	≈0	0.78	0	0	0	2.6
	1 pu	1.6 - 2.0	0	0.76	0	0	0	2
	1 pu	1.6 - 2.0	0	0.76	0	0	0	2
	1 pu	1.6 - 2.0	0	0.75	0.04	0.04	0	2.8
	1 pu	1.6 - 2.0	0	0.75	0.02	0.02	0	3
	1 pu	1.6 - 2.0	0	0.75	0.02	0.02	0	2.8
	1 pu	1.6 - 2.0	0	0.76	0	0	0	2.4
	1 pu	1.6 - 2.0	0	0.76	0	0	0	2.4
	1 pu	1.6 - 2.0	≈0	0.78	0.6	0	0	2.4
IEEE 37.118			1%		0.005	0.01 Hz/s		

5.2. Magnitude Test

The subsequent range, 0.8 to 1.6 seconds, depicts dynamic grid conditions, magnitude error, and frequency ramp, with the CC varying from −1 to +1. In this region, the maximum TVE is 0.595%, as specified in IEEE 37.118 standards. The TVE remains between 0% and 1.2%, which is below the IEEE 37.118 standard limit of 0.595% for dynamic step conditions. The correlation coefficient (CC) oscillates between 1 and −1, where a negative CC indicates phase reversal after a step change, *i.e.*, (π rad or 180-degree phase shift). The Frequency Error (FE), ranging from 0 to 0.6 Hz, complies with IEEE 37.118 standards for dynamic response. The RFE and FE show similar magnitudes, mainly due to the lack of sudden frequency spikes, measured between 0 and 0.6 Hz/s for the RFE. The Phasor Magnitude remains constant at 100 pu, and the PAE oscillates up to ±π radians, as expected for the magnitude step test. Negative CC values indicate polarity reversals (phase shifts of approximately π rad), and FE demonstrates that the PMU handles significant phase jumps without exceeding frequency error limits. In conclusion, the DFT-ADALINE algorithm fulfills IEEE requirements for step change magnitude, FE, and RFE.

5.3. GPS Failure Test

The GPS failure tests show that the TVE is nearly zero, indicating that magnitude

and phasor tracking did not significantly drift despite the GPS failure. However, the Correlation Coefficient (CC) ranged from 0.75 to 0.78, which is below 1, confirming that the GPS is not locked to the PMU. The FE and RFE are minimal values, such as 0.02 and 0.04 Hz, caused by degraded timing accuracy. The Phasor Magnitude is zero, and the PAE ranged between 2 and 2.8. The results for FE, RFE, TVE, Phasor Magnitude, PAE, and CC confirm a loss of synchronization. The phase angle instability suggests that the PMU is operating without GPS. Since the CC is less than 1, it indicates that the PMU would not pass the IEEE compliance test. Including the RTC in the final PMU design helps compensate for the GPS failure in the prototype.

6. Limitations of the Study

This study faced several limitations that should be acknowledged. The DFT-ADALINE algorithm was run on theoretical microcontrollers imbedded in MATLAB/Simulink in which the microcontroller processing latency that is likely to occur in the prototype was not analyzed. Further, we were unable to simulate real noise experience of the power grid in MATLA/Simulink to precisely assess the performance of the DFT-ADALINE algorithm. Despite these limitations, the performance of the algorithm against the power grid conditions that were simulated was within the prescribed thresholds of the IEEE 37.118 standards.

7. Conclusions

In conclusion, the DFT-ADALINE algorithm meets the IEEE standards for step change magnitude, FE, and RFE. The minor PAE adjustments align with the expected phase shift during frequency ramps, and the High CC indicates excellent tracking performance. During the frequency ramp test, the CC stayed at one, which perfectly matches the values obtained for FE, RFE, Phasor Magnitude, PAE, and TVE.

Furthermore, for the magnitude test, the CC is set to 1 under normal grid operating conditions and −1 during abnormal grid conditions, which aligns with the values obtained for the FE, RFE, Phasor Magnitude, PAE, and TVE.

Finally, the CC is below 0.78 for the GPS signal loss, which corresponds with the out-of-range values for the FE, RFE, Phasor Magnitude, PAE, and TVE.

The results from **Figure 22** show that CC values between 0.8 and 1 indicate normal grid operating conditions, while those below 0.8 indicate abnormal conditions. Therefore, the CC can be used as a single reference measurement to predict grid operation in dynamic situations. This finding is useful for implementing the PMU in the power system's distribution network, where operating conditions are highly variable. It simplifies monitoring by reducing the number of control parameters needed to assess the grid's state and provides a clear indicator for determining operational conditions.

This study shows how a single PMU measurement parameter, the correlation coefficient, can predict the behavior of the power grid under dynamic conditions

and be used to trigger adjustments to grid voltage and frequency. It also greatly simplifies the fault detection logic of the power system and cuts down on computation delays.

It is recommended to implement the DFT-ADALINE on hardware to test its performance in a real power system environment.

Conflicts of Interest

The authors declare no conflicts of interest regarding the publication of this paper.

References

[1] Castello, P., Muscas, C., Pegoraro, P.A. and Sulis, S. (2019) Low-Cost Implementation and Characterization of an Active Phasor Data Concentrator. *ACTA IMEKO*, **8**, 21-27. https://doi.org/10.21014/acta_imeko.v8i2.625

[2] Vijaya Rama Raju, V., Phani Shree, K.H. and Jayarama Kumar, S.V. (2021) Development of Cost-Effective Phasor Measurement Unit for Wide Area Monitoring System Applications. *International Journal of Electrical and Computer Engineering* (*IJECE*), **11**, 4731-4739.

[3] Ndilimabakaa, H. and Blanc, I. (2014) Development of a Reference Phasor Measurement Unit (PMU) for the Monitoring and Control of Grid Stability and Quality. *EPJ Web of Conferences*, **77**, Article No: 9. https://doi.org/10.1051/epjconf/20147700009

[4] Wang, Y., Lu, C., Kamwa, I., Fang, C. and Ling, P. (2020) An Adaptive Filters Based PMU Algorithm for Both Steady-State and Dynamic Conditions in Distribution Networks. *International Journal of Electrical Power & Energy Systems*, **117**, Article ID: 105714. https://doi.org/10.1016/j.ijepes.2019.105714

[5] Perez, M.A., Betancourt, R.J. and Barocio, E. (2024) A Simplest Padé Approximant-Based Algorithm for Phasor Estimation of Electrical Signals. https://www.cinergiaug.org/assets/files/RIE_Vol.-7_No.2_202410.pdf

[6] Xu, S., Liu, H., Bi, T. and Martin, K.E. (2020) A High-Accuracy Phasor Estimation Algorithm for PMU Calibration and Its Hardware Implementation. *IEEE Transactions on Smart Grid*, **11**, 3372-3383. https://doi.org/10.1109/tsg.2020.2965195

[7] Leibovich, P., Issouribehere, F. and Barbero, J. (2018) Comparison of Synchrophasor Estimation Methods in Simulation Environment and Real Hardware Implementation. 2018 *IEEE Power & Energy Society General Meeting* (*PESGM*), Portland, 5-10 August 2018, 1-5. https://doi.org/10.1109/pesgm.2018.8585882

[8] Musonda, G., Lubobya, C. and Zulu, A. (2025) Adaptive Artificial Neural Network (ADALINE) Dynamic Phase Error Estimation Based on the Average Correlation Coefficient. *World Journal of Engineering and Technology*, **13**, 440-461. https://doi.org/10.4236/wjet.2025.133028

[9] Deepa, B., Hampannavar, S. and Mansani, S. (2024) Phasor Estimation Using Micro-Phasor Measurement Unit (μPMU) in Distribution Network for Situational Awareness. *Journal of Electrical Systems and Information Technology*, **11**, Article No. 52. https://doi.org/10.1186/s43067-024-00179-5

[10] Alghamdi, H.A., Adham, M.A., Farooq, U. and Bass, R.B. (2025) Enhancing Frequency Event Detection in Power Systems Using Two Optimization Methods with Variable Weighted Metrics. *Energies*, **18**, Article 1659. https://doi.org/10.3390/en18071659

[11] Delle Femine, A., Gallo, D., Landi, C. and Luiso, M. (2019) The Design of a Low Cost

Phasor Measurement Unit. *Energies*, **12**, Article 2648.
https://doi.org/10.3390/en12142648

[12] Li, H. (2019) Frequency Estimation and Tracking by Two-Layered Iterative DFT with Re-Sampling in Non-Steady States of Power System. *EURASIP Journal on Wireless Communications and Networking*, **2019**, Article No. 28.
https://doi.org/10.1186/s13638-018-1320-1

[13] Chen, L., Zhao, W., Wang, F., Yu, Y. and Huang, S. (2019) Dynamic Synchrophasor Estimation Algorithm for P-Class Phasor Measurement Units. 2019 *IEEE Milan PowerTech*, Milan, 23-27 June 2019, 1-6. https://doi.org/10.1109/ptc.2019.8810925

[14] Ponnala, R., Chakravarthy, M. and Lalitha, S.V.N.L. (2022) Novel PMU Model for Dynamic State Disturbance Analysis with Effective Data Handling System. *International Journal of Electrical and Electronics Research*, **10**, 1306-1314.
https://doi.org/10.37391/ijeer.100485

[15] Feng, H. and Sun, L. (2024) Design and Simulation of Butterworth Low-Pass Filter. *Academic Journal of Science and Technology*, **10**, 106-110.
https://doi.org/10.54097/jpnnb366

[16] Tüzün, R. and Akçam, N. (2018) Design of Microstrip Low Pass Filters. 6*th International Symposium on Innovative Technologies in Engineering and Science*, Antalya, 9-11 November 2018.

[17] Liu, M., Liu, Y., Wang, Y., Dinavahi, V. and Gao, Z. (2025) Robust Dynamic State Estimation of Power System with Measurement Outliers Based on Parameterized Analytical Cubature Kalman Filter. *IET Renewable Power Generation*, **19**, e70047.
https://doi.org/10.1049/rpg2.70047

[18] Ulloa, H.C., Vel'asquez, G.I. and Guingla, D.P. (2018) The Extended Kalman Filter in the Dynamic State Estimation of Electrical Power Systems. *Enfoque UTE*, **9**, 120-130.

[19] Gao, Z., Li, C., Tian, C., Wang, Y., Pan, X., Zhang, G., *et al.* (2025) Resilient Dynamic State Estimation for Power System Based on Modified Cubature Kalman Filter against Non-Gaussian Noise and Outliers. *Electronics*, **14**, Article 2430.
https://doi.org/10.3390/electronics14122430

[20] Jan Kikkert, C. (2019) A Phasor Measurement Unit Algorithm Using IIR Filters for FPGA Implementation. *Electronics*, **8**, Article 1523.
https://doi.org/10.3390/electronics8121523

[21] Elsayed, A.A., Abdellah, M.A., Mohamed, M.A. and Nayel, M.A.E. (2022) UPMU Hardware and Software Design Consideration and Implementation for Distribution Grid Applications. *Advances in Science, Technology and Engineering Systems Journal*, **7**, 59-71. https://doi.org/10.25046/aj070409

[22] Zhang, J., Tang, C., Liu, C., Wang, H., Junfeng, D. and Tang, S. (2023) Phasor Measurement Method Based on Soft Synchronized Sampling with Temporal Pulse Signal Reference. *Frontiers in Energy Research*, **11**, Article 1302869.
https://doi.org/10.3389/fenrg.2023.1302869

[23] Brogan, P.V., Laverty, D.M., Zhao, X., Hastings, J., Morrow, D.J. and Vanfretti, L. (2018) Technique for Pre-Compliance Testing of Phasor Measurement Units. *International Journal of Electrical Power & Energy Systems*, **99**, 323-330.
https://doi.org/10.1016/j.ijepes.2018.01.031

[24] Zhan, L.W., Liu, Y. and Liu, Y.L. (2015) A Clarke Transformation-Based DFT Phasor and Frequency Algorithm for Wide Frequency Range. *IEEE Transactions on Smart Grid*, **9**, 67-77.

[25] Garanayak, P. and Panda, G. (2016) Fast and Accurate Measurement of Harmonic

Parameters Employing Hybrid Adaptive Linear Neural Network and Filtered-X Least Mean Square Algorithm. *IET Generation*, *Transmission & Distribution*, **10**, 421-436. https://doi.org/10.1049/iet-gtd.2015.0684

[26] Garanayak, P., Panda, G. and Mishra, S. (2018) Harmonic Elimination Using SW Based HSAPF System and Evaluation of Compensation Effect Employing ADALINE-DFFRLS Algorithm. *EPE Journal*, **29**, 64-81. https://doi.org/10.1080/09398368.2018.1483118